

# NJC

Accepted Manuscript



This article can be cited before page numbers have been issued, to do this please use: Y. Arakawa, K. Komatsu and H. Tsuji, *New J. Chem.*, 2019, DOI: 10.1039/C8NJ06456C.



This is an Accepted Manuscript, which has been through the Royal Society of Chemistry peer review process and has been accepted for publication.

Accepted Manuscripts are published online shortly after acceptance, before technical editing, formatting and proof reading. Using this free service, authors can make their results available to the community, in citable form, before we publish the edited article. We will replace this Accepted Manuscript with the edited and formatted Advance Article as soon as it is available.

You can find more information about Accepted Manuscripts in the [author guidelines](#).

Please note that technical editing may introduce minor changes to the text and/or graphics, which may alter content. The journal's standard [Terms & Conditions](#) and the ethical guidelines, outlined in our [author and reviewer resource centre](#), still apply. In no event shall the Royal Society of Chemistry be held responsible for any errors or omissions in this Accepted Manuscript or any consequences arising from the use of any information it contains.

NJC

ARTICLE

## Twist-bend nematic liquid crystals with thioether linkages

Yuki Arakawa,\* Kenta Komatsu, and Hideto Tsuji

Received 00th January 20xx,  
Accepted 00th January 20xx

DOI: 10.1039/x0xx00000x

www.rsc.org/

We developed twist-bend nematogens based on cyanobiphenyl dimers with thioether or sulfur linkages, as opposed to the commonly used methylene and ether linkages. Based on the smaller bond angle of thioether C-S-C than methylene C-CH<sub>2</sub>-C and ether C-O-C, we designed two dimer homologous series that are more bent, symmetric CBSnSCB with two thioether linkages and asymmetric CBSnOCB with a thioether and ether linkage, containing odd carbon numbers  $n = 3, 5, 7, 9$ , and  $11$ , and also synthesized even- $n$  members  $n = 6$  for each system. Both CBSnSCB with  $n = 3, 5$  and  $7$  and CBSnOCB with  $n = 5$  and  $7$  formed a broad range of twist-bend nematic phases that were stable down to room temperature and showed remarkably enhanced glass-forming ability. DFT calculations revealed that twist-bend nematogens CBS7SCB and CBS7OCB have smaller bend angles made of the para axes of the two cyanobiphenyl moieties and larger dipole moments than those of conventional nematogen ether-linked CBO7OCB.

### Introduction

Molecular geometry or shape plays an important role in liquid crystals located between three-dimensional solid crystals and isotropic (I) liquids. In 2001, Dozov predicted the possibility of a unique helical-nanostructured nematic (N) phase with conical director distribution along its helical axis for bent-shaped mesogens, referred to as twist-bend nematic ( $N_{TB}$ ) phase [1]. In experimental research, the N to another undefined N ( $N_x$ ) transition was initially observed for bent dimers with different odd-numbered alkylene spacers [2]. Then, Cestari et al. revealed that, based on <sup>2</sup>H-NMR measurement using a deuterated achiral dimer with  $N_x$  transition, a chiral structure or symmetry breaking was generated in the  $N_x$  phase, and then, the  $N_x$  phase was identified as the  $N_{TB}$  phase [3]. The periodic formation has been observed by freeze-fracture transmission electron microscopy [4] and scanning electron microscopy based on photo-polymerized materials [5]. Recently, resonant carbon *K*-edge soft X-ray scattering measurement [6] has revealed that the local director is tilted against its helix axis and the helix pitch is close to 10 nm in the  $N_{TB}$  phase [6a,b]), and that it also supports the double helix formation in the  $N_{TB}$  phase [6b,c)] proposed previously [7]. From the view point of molecular design, furthermore, there is the fact that a duplexed hexamer forms a wider  $N_{TB}$  phase than the one parent trimer, sustaining such a double helical structure formed in  $N_{TB}$  phase [8].

Inspired by the recent discovery of the  $N_{TB}$  phase, the development of new twist-bend nematogens has been a

significant focus of research on liquid crystals and condensed matter. In addition to low-molecular-weight molecules, twist-bend nematogens have been found for oligomers [9] as well as polymers [10]. Twist-bend nematogens are expected to have new applications owing to their fast electrooptical response [11] and helicoidal cholesteric structure [12]. In addition, the twist-bend smectic phase has recently been discovered [13].

Some methylene-linked cyanobiphenyl dimers (CB<sub>n</sub>CB - wherein CB refers to cyanobiphenyl units and  $n$  denotes the odd carbon number in the alkylene spacer), form the enantiotropic  $N_{TB}$  phase [3-6,14], in which the first report for CB<sub>n</sub>CB postulated the  $N_x$  or  $N_{TB}$  phase as a smectic A phase [15]. Although the ether-linked counterparts CBO<sub>m</sub>OCB are recognized as conventional nematogens [16], a recent in-depth analysis by Paterson et al. indicated that CBO5OCB forms a narrow monotropic  $N_{TB}$  phase range [17]. Sebastián et al. reported that some dual ether-linked fluorinated CB dimers are capable of forming kinetically-dependent  $N_{TB}$  phase with a broad range [18]. On the other hand, Mandle et al. have explored the structure-property relationship extensively for the development of twist-bend nematogens [19]. They reported that not only the structures of mesogenic parts but also the bend angles made by the para axes of the two mesogenic moieties are essential determinants of the formation of the  $N_{TB}$  phase. Moreover, they found that ether linkages are less likely to induce the  $N_{TB}$  phase alongside methylene linkages due to the larger bond angle for C-O-C than C-CH<sub>2</sub>-C, making the molecular geometry of ether-linked dimers close to a straight rod shape. Accordingly, it is interesting to note that the asymmetrically methylene- and ether-linked cyanobiphenyl dimers CB6OCB [20] and CB8OCB [18b]) form monotropic  $N_{TB}$  phases. Dawood et al. reported that a Schiff base dimer with a propylene spacer forming  $N_{TB}$  phase transitioned directly from the I phase without an intermediate N phase, in which the molecular design is based

Department of Environmental and Life Sciences, Graduate School of Engineering, Toyohashi University of Technology, 1-1 Hibiyaoka, Tempaku-cho, Toyohashi, Aichi 441-8580, Japan. E-mail: ya017@edu.tut.ac.jp.

\* Footnotes relating to the title and/or authors should appear here.

Electronic Supplementary Information (ESI) available: [details of any supplementary information available should be included here]. See DOI: 10.1039/x0xx00000x

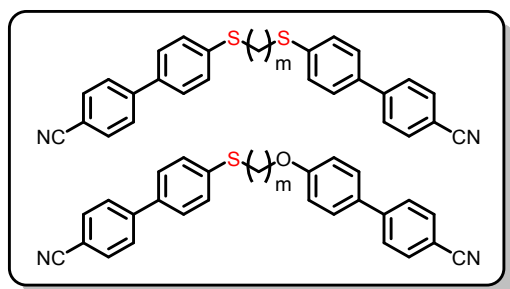


Fig. 1. Molecular structures of the thioether-linked dimers CBSnSCB and CBSnOCB.

on the theory that postulates more bent structures for shorter spacer dimers [21]. Furthermore, Jansze et al. and Walker et al. found that hydrogen-bonded oligomers based on non-twist-bend nematogenic or non-mesogenic molecules also work as twist-bend nematogens [22]. Thus, a large variety of twist bend nematogenic dimers or oligomers has recently been developed. Nevertheless, the inserted linking atoms between a mesogenic part and a spacer for twist-bend nematogens are typically based exclusively on carbon, followed by oxygen.

This study presents, for the first time, twist-bend nematogens based on thioether (C-S-C)-linked dimers, that is, sulfur is included in the linking atom. So far, we have been addressing the development of thioether-containing rod-like mesogens [23], wherein we noted the bond-angle features for the smaller bond angle of ca. 100° for C-S-C in thioether than ca. 118° for C-O-C in ether and ca. 110° for C-CH<sub>2</sub>-C in alkylene. In the light of such a small bond angle of thioether, then, we perceived that a thioether linkage could be preferable to induce a more-bent molecular curvature geometry. Herein, we designed two dimer families that are more bent; symmetric CBSnSCB with two thioether linkages and asymmetric CBSnOCB with a thioether and ether linkage, with carbon numbers n = 3, 5, 7, 9, and 11 (Fig. 1). In the acronyms CBSnSCB and CBSnOCB, S and O respectively indicate the thioether and ether linkages. In addition, even members CBS6SCB and CBS6OCB, which are considered close to rod-like (or strictly Z-shaped) molecular geometry, were also prepared.

## Experimental

All chemicals were purchased from commercial suppliers as depicted in ESI and used without further purification. The synthetic routes for CBSnSCB and CBSnOCB are shown in Fig. 2. Both homologous series were synthesized through a Williamson ether reaction between 4-bromobenzenethiol or 4-bromophenol and corresponding  $\alpha,\omega$ -dibromoalkanes, and a Suzuki-Miyaura coupling reaction [24]. Their respective characterization data are described in ESI.

Molecular structures were characterized by <sup>1</sup>H NMR and <sup>13</sup>C NMR measurements on a JEOL LNM-EX 400 and a Bruker Avance III 400, respectively. The phase transitions were investigated by polarizing optical microscopy (POM) (BX50, Olympus) with a temperature controller (LK-600PM, Linkam Scientific Instruments) and differential scanning calorimetry (DSC) (DSC-

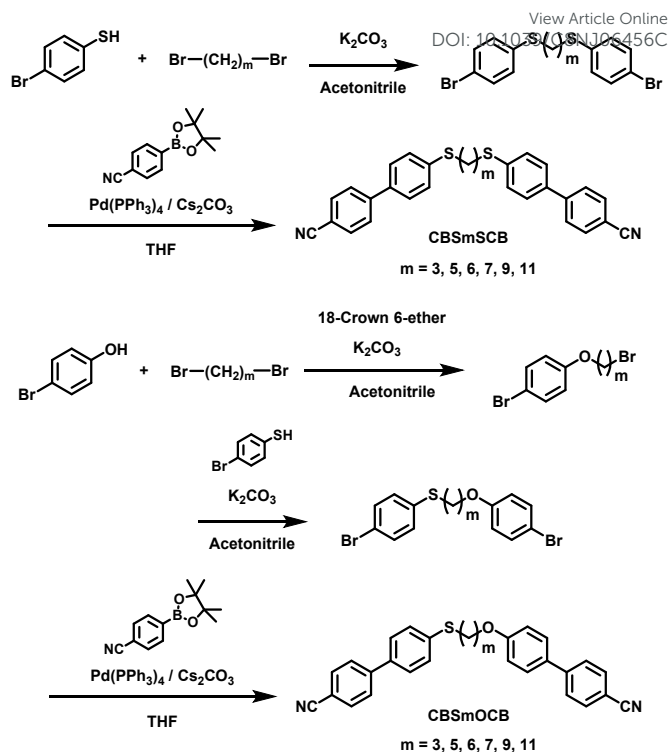


Fig. 2. Synthetic routes of CBSnSCB and CBSnOCB.

60, Shimadzu) with heating and cooling scans performed at a rate of 3 °C min<sup>-1</sup> under nitrogen gas. CBS3SCB, CBS7SCB and CBS7OCB were subject to further DSC measurements on a DSC 8500 (Perkin Elmer) equipped with an Intracooler II at different rates under nitrogen gas. X-ray diffraction (XRD) measurements were conducted using a Bruker D8 DISCOVER equipped with a Vantec-500 detector using Cu-K $\alpha$  radiation. The specimens, kept in capillary glass tubes of 1.5 mm diameter (purchased from WJM-Glass Müller GmbH), were aligned under a magnetic field (B = 1 T). In order to estimate the molecular parameters including molecular conformation, dipole moment, and charge distribution for the optimized molecular geometries, density functional theory (DFT) calculations were used. Molecular structure optimization was carried out using Gaussian 16 [25] with the spacer in the all-trans conformation at the B3LYP/6-31G(d) level of theory [26]. For visualization and analysis of the calculated results, Gauss View 6 [27] was used.

## Results and Discussion

The mesomorphic behaviors of CBSnSCB and CBSnOCB were evaluated by a combination of POM and DSC. Upon heating, almost all the homologs, with the exception of CBS3SCB, CBS5SCB, and CBS6SCB, showed only conventional N phases; their phase transition behavior is summarized in Table S1. As a representative result, the N phase had a wider range of ca. 25 °C for CBS7OCB compared with ca. 4 °C for CBS7SCB.

The phase sequences, transition temperatures and enthalpy changes upon cooling are listed in Table 1. POM observation for CBS7SCB was performed in uniaxially planar-aligned polyimide-

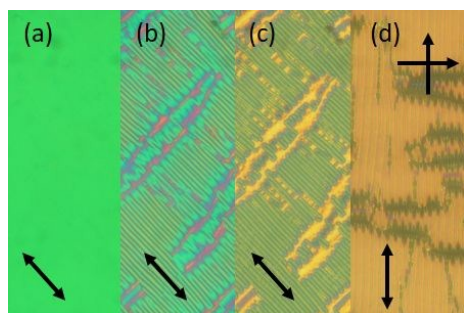


Fig. 3. Photomicrographs of CBS7SCB for the N phase at 100 °C (a), for the  $N_{TB}$  phase at 85 °C (b) and 50 °C (c) and (d). Crossed arrows and lower arrows represent polarizers and rubbing directions, respectively.

Table 1. Phase transition temperature (°C) and enthalpy changes ( $\text{kJ mol}^{-1}$ ) at a rate of 3 °C  $\text{min}^{-1}$  upon cooling.

Sample	Phase sequence
CBS3SCB	$N_{TB}$ 44 (-) <sup>a</sup> Cr 63.9 (11.9) <sup>b</sup> N 83.1 (0.2) I
CBS5SCB	Cr 76.6 (19.9) <sup>b</sup> $N_{TB}$ 78 (-) <sup>a</sup> N 107.7 (0.7) I
CBS6SCB	Cr 186.5 (61.6) I
CBS7SCB	G 15.9 $N_{TB}$ 88.3 (0.3) N 115.2 (1.4) I
CBS9SCB	Cr 100.8 (33.4) N 116.7 (2.4) I
CBS11SCB	Cr 101.4 (42.0) N 114.4 (3.0) I
CBS3OCB	Cr 101.1 (25.4) N 137.4 (0.66) I
CBS5OCB	Cr 76.6 (17.0) <sup>b</sup> $N_{TB}$ 90.1 (0.04) N 143.5 (1.4) I
CBS6OCB	Cr 176.7 (49.2) N 191.3 (7.8) I
CBS7OCB	Cr 55.0 (16.7) <sup>b</sup> $N_{TB}$ 95.9 (0.06) N 146.7 (2.0) I
CBS9OCB	Cr 98.0 (36.3) N 143.0 (2.1) I
CBS11OCB	Cr 102.5 (37.4) N 134.1 (2.9) I

<sup>a</sup> Observed by POM, <sup>b</sup> Imperfect crystallization.

surface cells with a cell thickness of 3  $\mu\text{m}$ ; representative photomicrographs are shown in Fig. 3. Figure 3(a) shows the N phase at 95 °C with a single green birefringent texture securing its uniaxial alignment. It should be noted that at 86 °C, the line along the rubbing direction gradually emerges, resulting in a stripe texture, as shown in Figs. 3(b)–(d). This textural behavior strongly suggests the emergence of the  $N_{TB}$  phase. The optical texture was not altered by the transition to crystal phases by cooling to ambient temperature. We found that CBSnSCB with  $n = 3, 5, 7$  and CBSnOCB with  $n = 5, 7$  show monotropic  $N_{TB}$  phases after the conventional N phase (Figs. S5–S8). This is the first report of thioether-linked twist-bend nematogens that include linking atoms other than carbon and oxygen. Combined with the fact that ether-linked CBOOCB dimers are mostly a conventional nematogen [16], the results for asymmetric CBS5OCB and CBS7OCB highlight the benefits of a thioether linkage for inducing the  $N_{TB}$  phase. Since the mesogenic behavior for the shortest spacer CBS3SCB strongly relies on kinetics and its N- $N_{TB}$  phase transition is preceded by crystallization at ca. 64 °C, we captured its  $N_{TB}$  phase by POM observation as shown in Fig. S8. Although a Schiff base dimer with a propylene spacer formed  $N_{TB}$  phase transitioned directly from I phase [21], it exhibited conventional sequences;  $N_{TB}$ -N-I

phases. On the other hand, although CBS3OCB showed just one melting peak at 142.9 °C without any mesophases upon the first heating, it formed N phase after the melt at 120.2 °C upon the second heating; it has a polymorph depending on the crystallization conditions. It is interesting to note that CBS3SCB also formed  $N_{TB}$  phase, but CBS3OCB did not, at a rate of 3 °C  $\text{min}^{-1}$ .

In marked contrast with mesogenic odd CBSnSCB members, an even CBS6SCB member, that is thought of as a straight rod shape, does not show any mesophases. This is thought to be due to the steric hindrance derived from the less bond angle [23] and rotational energy barrier [28] for thioether, disturbing the mesophase formation for rod-shaped molecules [23]. This suggests that dimeric curvature on the basis of thioether has a beneficial effect in the mesogenic induction. CBS6OCB forms enantiotropic N phase. Both even members show drastically higher transition temperatures and associated enthalpy changes compared with odd ones, reflecting the difference of each molecular geometry.

We plotted the transition temperatures at N-I [ $T(NI)$ ] and  $N_{TB}$ -N [ $T(N_{TB}N)$ ] against  $n$  for both odd- $n$  members in Fig. 4. One can see that the  $T(NI)$  values are wholly lower for sole thioether-containing CBSnSCB than for ether-containing CBSnOCB. This is similar to the trend observed for the calamitic mesogens with each alkylthio and alkoxy group, which is ascribed to the steric hindrance due to the smaller bond angle and lower rotation barrier for the former than the latter. In the present case for bent dimers, the  $T(NI)$  depression for sole thioether-containing CBSnSCB are attributed to the more bent molecular geometry compared to CBSnOCB as discussed later in DFT calculations. The  $T(NI)$  values slightly ascend with an increasing carbon number and then reaches the maxima at the middle length. The  $T(N_{TB}N)$  values also increase with an increasing carbon number within the twist bend nematogens, resulting in the wider range of  $N_{TB}$  phases. Here, it is interesting to note that although CBSnSCB form narrower N phases than CBSnOCB, the former has wider  $N_{TB}$  ranges than the latter, in a case where kinetically preceded crystallization is not considered. Wholly, the observed trends are consistent with molecular field theory for V-shaped nematogens; As the molecular bend angle decreases from 140° or more bent geometry, its uniaxial N ( $N_U$ ) phase region decreases by the  $T(NI)$  decrement and incidence of biaxial N ( $N_B$ ) phase or the  $N_{TB}$  phase, giving rise to a widened region for the latter phases [29], wherein a certain bend angle further close to 90° contributes to stabilize  $N_U$  again or destabilize  $N_B$  or  $N_{TB}$  phases.

In addition, we estimated the entropy changes ( $\Delta S$ ) scaled by gas constant ( $R$ ) at  $N_{TB}$ -N transition [ $\Delta S(N_{TB}N)/R$ ] and at N-I transition [ $\Delta S(NI)/R$ ], with which the latter are listed in Table S2 and plotted in Fig. 5.  $\Delta S(N_{TB}N)/R$  of 0.30 for CBS7SCB is larger than 0.04 for CBS5OCB and 0.06 for CBS7OCB and similar to 0.31 for CB7CB [3]. Whilst,  $\Delta S(NI)/R$  values are determined as 0.42 for CBS7SCB and 0.57 for CBS7OCB which is not so much different from 0.34 for CB7CB [3,14] and 0.66 for CBO7OCB [15a)]. As can be seen in Fig. 5, the  $\Delta S(NI)/R$  values linearly correlate with  $n$  in odd members for both systems. Based on the slope of the plots, the increase in  $\Delta S(NI)/R$  per ethylene ( $-\text{CH}_2-$

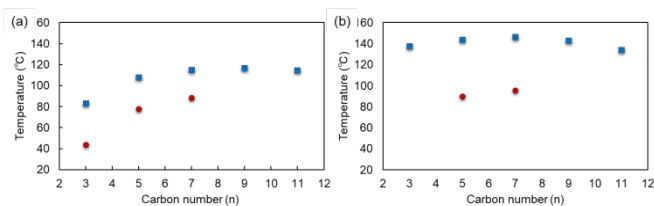


Fig. 4. The transition temperatures at N<sub>TB</sub>-N (circle) and N-I (square) as a function of odd spacer number *n* for CBSnSCB (a) and CBSnOCB.

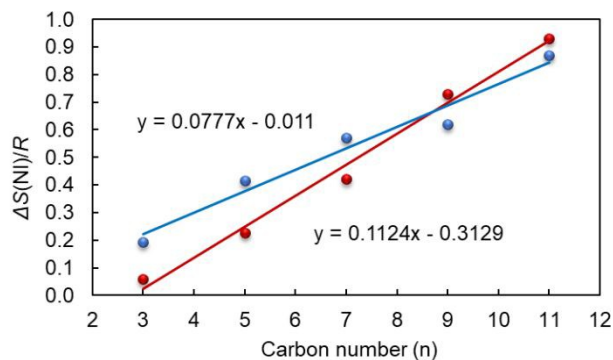


Fig. 5. The plots of  $\Delta S(NI)/R$  values for CBSnSCB (circle) and CBSnOCB (square) as a function of carbon number in the odd spacer.

CH<sub>2</sub>-) is estimated as 0.11 for odd-*n* CBSnSCB and 0.08 for odd-*n* CBSnOCB, respectively, leading to the estimation of its increase of ca. 0.1 per an ethylene spacer for odd-spacer dimers. It seems that  $\Delta S(NI)/R$  values are smaller for CBSnSCB than for CBSnOCB in short spacer dimers, but they inversely become similar or slightly larger for the former than the latter in long spacer dimers above *n* = 9. This may be attributed to the speculation; short-spacer dimers reflect the bent molecular geometry but long-spacer ones give rise to deviation from bent geometry due to more conformers and the dilution effect of mesogenic parts, in each mesophase [21]. Accordingly, CBSnSCB would show the lower and similar or slightly higher values than CBSnOCB in small and large *n*, respectively.

CBS7SCB was subjected to further DSC measurements at different heating and cooling rates of 1, 3, and 10 °C min<sup>-1</sup>, as depicted in Fig. 6. At any given cooling rate, the transition from the N phase to N<sub>TB</sub> phase was discernible. Subsequently, the N<sub>TB</sub> phase was supercooled to room temperature, and the glass transitions were observed at ca. 16 °C without crystallization at a conventional rate of 10 °C min<sup>-1</sup>. Even at slower rates of 1 and 3 °C min<sup>-1</sup>, a partially crystallized glassy state was observed, which is supported by the existence of the glass transition and double cold-crystallization upon subsequent heating, as shown in Fig. S9. CBS3SCB, CBS5SCB, CBS5OCB, and CBS7OCB are also capable of being vitrified with partial crystallization at a rate of 3 °C min<sup>-1</sup>.

N<sub>TB</sub> phases that are stable down to room temperature are highly rare [30]. The representative methylene-linked CB7CB [14a]) and CB9CB [14b]) show low glass transition temperatures under 10 °C and require a high cooling rate of over 30 °C min<sup>-1</sup> to be vitrified with partial crystallization. In addition, the

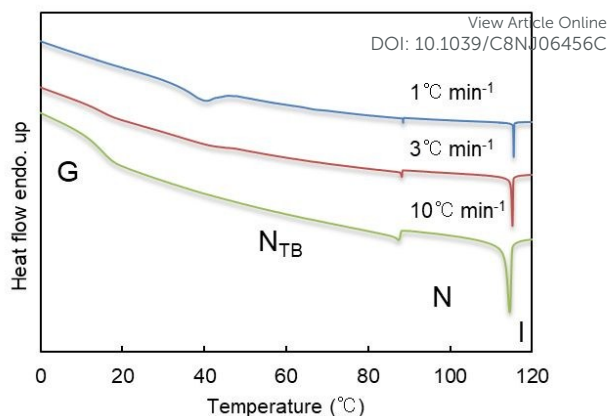


Fig. 6. DSC curves for CBS7SCB upon cooling after heating. G: glass, Cr: crystal, N: nematic phase, and I: isotropic phase.

asymmetrically methylene- and ether-linked monotropic twist bend nematogens CB6OCB [20] and CB8OCB [19b]) crystallized at the given rates. The present results suggest that a thioether linkage prevents crystallization and enhances the glass-forming ability for bent-dimeric mesogens, allowing us to easily keep the desirable molecular aggregation states. Intriguingly, this runs counter to the fact that highly polarizable thioether-containing rod-like mesogens have an intrinsically stronger crystallization ability due to stronger intermolecular attractive interactions than those of their alkyl and alkoxy counterparts [23].

Next, CBS7SCB and CBS7OCB were used to obtain temperature-dependent XRD measurements in a magnetic field (*B* = 1 T). The 2D- and 1D-XRD patterns for CBS7SCB are shown in Figs. 7(a)–(c), wherein the long molecular axis corresponds to the magnetic field direction represented by an arrow. In the small-angle region, subtle diffraction reminiscent of molecular clusters was observed. The *d*-spacings were ca. 13 Å (Table S3 and Fig. S14), which were close to half of the length of each molecule. Traditionally, it is known that nematogenic dimers often show X-ray diffraction associated with close to or less than a molecular half length. Although it has been ascribed to their intercalated structures in a molecular cluster, such a model yet requires further careful discussion. Here, it is curious that the small-angle diffraction intensities become rather low after the transition to the N<sub>TB</sub> phase from N phase and a similar behavior is observed for CBS7OCB (Figs. S12 and S13). Salamończyk et al. reported that the presence and absence of the resonant X-ray scattering corresponding to a full and half pitch of a helix in an N<sub>TB</sub> phase, respectively, suggests the two interlocked and shifted double helices [6b]). Based on the above knowledges, the present results may reflect such a change of the local molecular clusters formed in the N and N<sub>TB</sub> phases, so as to form shifted double-helical structures in the latter.

We estimated their orientational order parameters in each N phase based on the azimuthal intensity distribution centered at 2 $\theta$  = ca. 4.5 Å located on the equatorial line for CBS7SCB and CBS7OCB and compiled them in Table S3 and plotted in Fig. 7 (d). As is the case with conventional uniaxial N phases, the estimated *S* values for both molecules also show a gradual increase on declining temperature within the range between

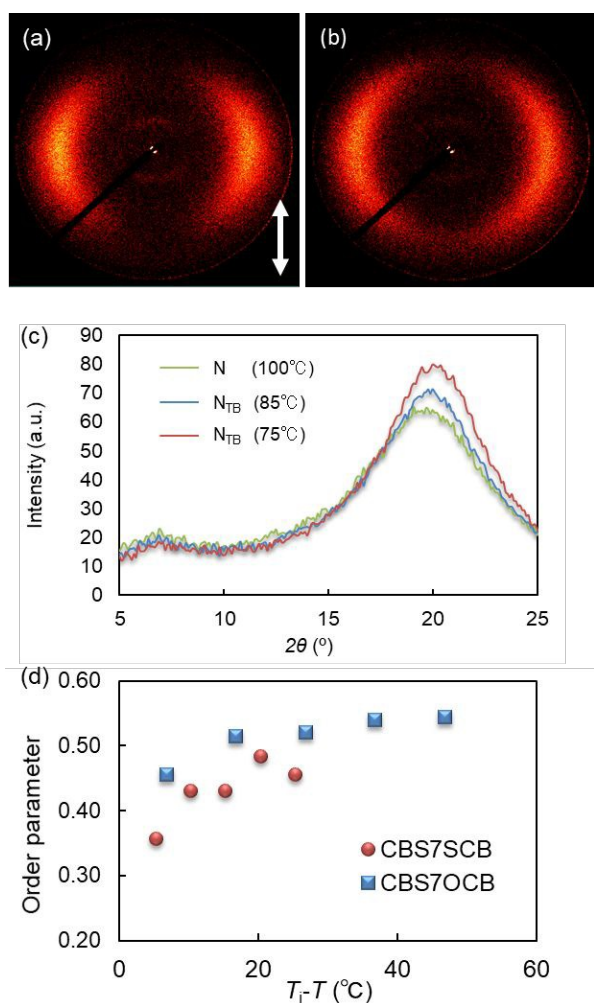


Fig. 7. 2D-XRD patterns of CBS7SCB for the N phase at 100 °C (a) and for the N<sub>TB</sub> phase at 85 °C (b), in which the long molecular axes are directed along each magnetic field direction, as indicated by arrows, 1D-XRD patterns for CBS7SCB (c), and temperature dependence of order parameters in each N phase for CBS7SCB and CBS7OCB based on the azimuthal intensity distribution of wide-angle diffraction centered at  $2\theta = \text{ca. } 4.5^\circ$  (d).

0.3 and 0.6, which is a natural consequence of the thermal fluctuations with respect to the director. Here, it is interesting to note that the orientational order parameters in each N phase were lower for CBS7SCB than for CBS7OCB, differing substantially from the propensity observed for thioether-containing rod-like mesogens, which tend to show higher order parameters than those of alkoxy counterparts due to enhanced intermolecular attractive interaction [23]. The present observation is an embodiment of the more bent geometry for the former than the latter in each N phase, as discussed later in DFT calculations. The lateral molecular distances evaluated from the wide-angle diffractions were smaller for CBS7SCB than for CBS7OCB at a similar reduced temperature (Table S2 and Fig. S10), implying the existence of effective intermolecular attractive interaction enhanced by two high-polarizable sulfur atoms.

As can be seen in Fig. 7(a) and (b), the orientation in the magnetic field became distinctly more disordered in the N<sub>TB</sub> phase than in the N phase. We fully understand that the discussion on the orientational order parameter in the N<sub>TB</sub>

phase needs careful explanation, since the fact that they increase with decreasing temperature is commonly accepted based on other methods; <sup>2</sup>H-NMR measurements using deuterated methylene linkages and para-axis of cyanobiphenyl parts in deuterated CBnCB [20,31] and Polarized Raman Spectroscopy [32]. Here, we will carefully consider about the origin of the broadened azimuthal intensity distribution of wide-angle X-ray diffraction in N<sub>TB</sub> phase. In the conventional N phase, molecules averagely uniaxially align along the magnetic field. In the N<sub>TB</sub> phase, whereas, molecules could form each helix with a tilt from its helical axis. Consequently, the azimuthal intensity distribution of a wide-angle diffraction could be expected to be wider than in the upper conventional N phase. Actually, Agra-kooijman et al. reported the plateau-like azimuthal intensity distribution of a wide-angle diffraction which can be individually fitted by gaussian equation, and is reminiscent of such a molecular tilt [33]. Then, they estimated that the tilt angle increases with decreasing temperature based on the wide-angle diffractions. In the present study, in addition, the obtained diffraction became further relaxed in the lower N<sub>TB</sub> region, making estimation of their order parameters rather difficult. In general, Helfrich-Hurault undulation (buckling) instability with undulated pseudo-layer structures as observed in smectic phases, resulting in the characteristic stripe and focal conic textures formed in N<sub>TB</sub> phases, is accepted for N<sub>TB</sub> phase [34]. The Helfrich-Hurault undulation instability model has a trend where the pitch declines with decreasing temperature. Such a broadened diffraction distribution or orientational relaxation in N<sub>TB</sub> phase may be attributed to not only molecular tilt but also helical tilt in undulations. Indeed, high-magnetic field like 25 T irradiation can achieve effective molecular alignment even in N<sub>TB</sub> phase [35] and the above described NMR measurements also usually used around 10 T. It seems that our condition of 1 T would not achieve the effective molecular orientation in N<sub>TB</sub> phase, which is similar to the previous reported XRD results using below 1.0 T [32, 36]. For reference, the order parameters estimated in each N<sub>TB</sub> phase with perhaps imperfect alignments are also given in Table S2 showing decreased values than those in each N phase. In addition, birefringence ( $\Delta n$ ) is also one of the major factors associated with the order parameter. Whereas,  $\Delta n$ -measurement in N<sub>TB</sub> phase is very hard due to the difficulty of obtaining sufficiently large and uniform N<sub>TB</sub> domains. Mayer et al. reported the precise measurement of the birefringence of CB7CB from its alternating double-generated single domains with opposite handedness in the N<sub>TB</sub> phase [37]. Wherein, they showed that the  $\Delta n$  once exhibits a positive jump and then suddenly decreased below the transition from N to N<sub>TB</sub> phase, which is an indicative of the macroscopic non-uniformity in N<sub>TB</sub> phase. They revealed that the tilt angle increases from 9° at N<sub>TB</sub>-N transition to saturated 37° with decreasing temperature based on  $\Delta n$  measurement. With respect to tilt angle, the NMR [31], XRD [33], PRS [34] and birefringence [37] measurements do not run counter to one another.

Finally, molecular geometries and electronic parameters for CBSnSCB and CBSnOCB were determined based on DFT calculations using Gaussian 16 and the basis function of

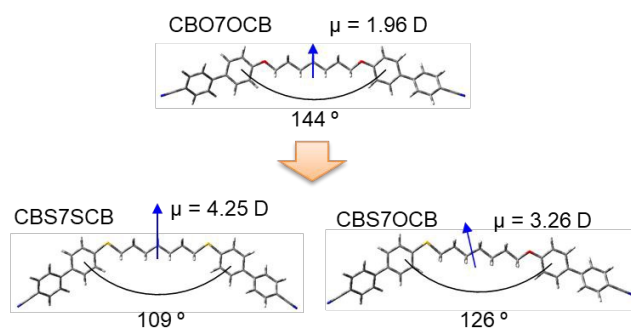


Fig. 8. Optimized molecular geometries and dipole moments (arrows) of conventional nematogen CBO7OCB, twist-bend nematogens CBS7SCB and CBS7OCB estimated based on DFT calculations at b3lyp/6-31g(d).

b3lyp/6-31g(d) [26]. As a reference, the DFT calculation was applied to conventional nematogen ether-linked CBO7OCB, too, which is consistent with the reported molecular bend values of 140° [19b)]. The optimized molecular structures for CBS7SCB, CBS7OCB and CBO7OCB are shown in Fig. 8. The estimated molecular bend angles, made of the para axes of the two cyanobiphenyl moieties in each system, were 109° for CBS7SCB and 126° for CBS7OCB. The bend angle for CBS7SCB was markedly smaller than, whereas that for CBS7OCB was highly similar to, the favorable value of 125° for twist-bend nematogens [19(b)]. Such more bent geometries for both systems are strongly ascribed to the bond angle of thioether linkages C-S-C estimated as ca. 103° since those for ether linkages of C-O-C were ca. 117°, by the present DFT calculations. It is clear that the dimers with a shorter spacer or a smaller bend angle have a tendency to form  $N_{TB}$  phase. This is ascribed to the fact that short-spacer dimers reflect the bent molecular geometry compared to long-spacer ones with more conformers and the dilution effect of mesogenic parts, resulting in a deviation from bent geometry. The inner benzene rings and the directly connected thioether linkages are coplanar with each other which is similar to the relationship for ether linkages but different from methylene linkages.

It is possible that such a bent geometry led by two thioether linkages for the former is not only more effective for the prevention of crystallization, as demonstrated by DSC, but also causes the mesogenic parts to deviate from the director, leading to the lower order parameter than that of the latter in each N phase, as determined by XRD. It should also be emphasized that thioether or alkylthio groups can present markedly contrasting phase transitions and mesogenic behaviors depending on the inherent molecular geometry between curves and rods [23]. In addition, their dipole moments are directed to molecular transverse axes, as shown in Fig. 8. Notably, the dipole moment value of 4.25 for CBS7SCB is larger than 3.26 for CBS7OCB, where both values are larger than the 1.96 for nematogen CBO7OCB (Fig. 8). This is achieved by the highly polarizable sulfur atom, and such laterally large dipole moments could also induce stable  $N_{TB}$  phases with high glass-transition temperatures for the present thioether-linked dimers. On the other hand, the sulfur atom in thioether has a positive charge

of 0.145, but ether-oxygen has a negative charge of -0.522. In addition, thioether has less electron donor properties than ether in the ground state [23,38], suggesting that they could have a considerable difference in their intermolecular interactions [23]. Accordingly, it can be concluded that the nature of the  $N_{TB}$  phase with an enhanced glass-forming ability for the present dimers can mainly be attributed to the synergistic effects of the largely-bent molecular geometry and high polarizability based on thioether.

## Conclusions

In summary, the results of this study offer a new molecular design and structural insight for the development of twist-bend nematogens based on thioether-linked dimers. In previous studies, twist-bend nematogenic dimers exclusively used carbon and oxygen in the linking atoms. As a result of the more bent dimeric curvature and high polarizability of thioether, the present dimers show a wide range of  $N_{TB}$  phases supercooled to room temperature and enhanced glass-forming ability. The present molecular designs lead to the facile synthetic method according to Williamson ether reaction to develop linkages. Furthermore, because of the intrinsically contained resonant sulfur atoms in the molecular structures, the present molecular design is expected to make it possible to apply the twist-bend nematogens to traditional resonant X-ray scattering at the sulfur  $k$ -edge without doping molecules with target resonant atoms [6c),39]. We will report the detailed phase-transition behavior, structural and physical properties of the present dimers, and design other thioether-linked twist-bend nematogens in future studies.

## Conflicts of interest

There are no conflicts to declare.

## Acknowledgments

This work was supported by KAKENHI 15H06285 and 17K14493, Toyota Physical and Chemical Research Institute Scholars, and the Naito Research Grant. We are grateful to Prof. Masatoshi Tokita for permission to use the instruments for DSC and temperature-variable XRD measurements.

## Notes and references

1. I. Dozov, *Europhys. Lett.*, 2001, **56**, 247.
2. (a) M. Šepelj, A. Lesac, U. Baumeister, S. Diele, H. L. Nguyen, D. W. Bruce, *J. Mater. Chem.*, 2007, **17**, 1154; (b) V. P. Panov, M. Nagaraj, J. K. Vij, Y. P. Panarin, A. Kohlmeier, M. G. Tamba, R. A. Lewis, G. H. Mehl, *Phys. Rev. Lett.*, 2010, **105**, 167801.
3. M. Cestari, S. Diez-Berart, D. A. Dunmur, A. Ferrarini, M. R. de La Fuente, D. J. B. Jackson, D. O. Lopez, G. R. Luckhurst, M. A. Perez-Jubindo, R. M. Richardson, J. Salud, B. A. Timimi, H. Zimmermann, *Phys. Rev. E*, 2011, **84**, 031704.

4. a) V. Borshch, Y. K. Kim, J. Xiang, M. Gao, A. Jakli, V. P. Panov, J. K. Vij, C. T. Imrie, M. G. Tamba, G. H. Mehl, O. D. Lavrentovich, *Nat. Commun.*, 2013, **4**, 2635; (b) D. Chen, J. H. Porada, J. B. Hooper, A. Klitnick, Y. Shen, M. R. Tuchband, E. Korblova, D. Bedrov, D. M. Walba, M. A. Glaser, J. E. Maclennan, N. A. Clark, *Proc. Natl. Acad. Sci. USA*, 2013, **110**, 15931.
5. V. P. Panov, S. P. Sreenilayam, Y. P. Panarin, J. K. Vij, C. J. Welch, G. H. Mehl, *Nano Lett.*, 2017, **17**, 7515.
6. a) C. Zhu, M. R. Tuchband, A. Young, M. Shuai, A. Scarbrough, D. M. Walba, J. E. Maclennan, C. Wang, A. Hexemer, N. A. Clark, *Phys. Rev. Lett.*, 2016, **116**, 147803; b) M. Salamończyk, N. Vaupotič, D. Pocięcha, C. Wang, C. Zhu, E. Gorecka, *Soft Matter*, 2017, **13**, 6694; c) M. Salamończyk, R. J. Mandle, A. Makal, A. Liebman-Peláez, J. Feng, J. W. Goodby, C. Zhu, *Soft Matter*, 2018, **14**, 9760.
7. a) R. J. Mandle, E. J. Davis, C. T. Archbold, C. C. Voll, J. L. Andrews, S. J. Cowling, J. W. Goodby, *Chem. Eur. J.*, 2015, **21**, 8158; b) M. R. Tuchband, M. Shuai, K. A. Graber, D. Chen, C. Zhu, L. Radzihovsky, A. Klitnick, L. M. Foley, A. Scarbrough, J. H. Porada, M. Moran, J. Yelk, D. Bedrov, E. Korblova, D. M. Walba, A. Hexemer, J. E. Maclennan, M. A. Glaser, N. A. Clark, 2017, arXiv:1703.10787.
8. R. J. Mandle, J. W. Goodby, *Angew. Chem. Int. Ed.*, 2018, **57**, 7096.
9. a) R. J. Mandle, J. W. Goodby, *ChemPhysChem*, 2016, **17**, 967; b) R. J. Mandle and J. W. Goodby, *RSC Adv.*, 2016, **6**, 34885; c) A. Al-Janabi, R. J. Mandle, J. W. Goodby, *RSC Adv.*, 2017, **7**, 47235.
10. a) D. A. Paterson, J. P. Abberley, W. T. A. Harrison, J. M. D. Storey, C. T. Imrie, *Liq. Cryst.*, 2017, **44**, 127; b) D. Stevenson, J. An, X.-B. Zeng, M. Xue, H.-X. Zou, Y.-S. Liu, G. Ungar, *Soft matter*, 2018, **14**, 3003.
11. a) V. P. Panov, R. Balachandran, M. Nagaraj, J. K. Vij, M. G. Tamba, A. Kohlmeier, G. H. Mehl, *Appl. Phys. Lett.*, 2011, **99**, 261903; b) C. Meyer, G. R. Luckhurst, I. Dozov, *Phys. Rev. Lett.*, 111, 067801.
12. a) J. Xiang, Y. Li, Q. Li, D. A. Paterson, J. M. D. Storey, C. T. Imrie, O. D. Lavrentovich, *Adv. Mater.*, 2015, **27**, 3014; b) J. Xiang, A. Varanytsia, F. Minkowski, D. A. Paterson, J. M. D. Storey, C. T. Imrie, O. D. Lavrentovich, P. Palffy-Muhoray, *Proc. Natl. Acad. Sci. USA*, 2016, **113**, 12925; c) Y. Wang, Z.-g. Zheng, H. K. Bisoyi, K. G. Gutierrez-Cuevas, L. Wang, R. S. Zola, Q. Li, *Mater. Horiz.*, 2016, **3**, 442.
13. J. P. Abberley, R. Killah, R. Walker, J. M. D. Storey, C. T. Imrie, M. Salamończyk, C. Zhu, E. Gorecka, D. Pocięcha, *Nature Commun.*, 2018, **9**, 228.
14. a) D. O. López, N. Sebastian, M. R. de la Fuente, J. C. Martínez-García, J. Salud, M. A. Pérez-Jubindo, S. Diez-Berart, D. A. Dunmur, G. R. Luckhurst, *J. Chem. Phys.*, 2012, **137**, 034502; b) B. Robles-Hernández, N. Sebastián, M. R. de la Fuente, D. O. López, S. Diez-Berart, J. Salud, M. B. Ros, D. A. Dunmur, G. R. Luckhurst, B. A. Timimi, *Phys. Rev. E*, 2015, **92**, 062505.
15. P. J. Barnes, A. G. Douglass, S. K. Heeks, G. R. Luckhurst, *Liq. Cryst.*, 1993, **13**, 603.
16. a) J. W. Emsley, G. R. Luckhurst, G. N. Shilstone, J. Sage, *Mol. Cryst. Liq. Cryst.*, 1984, **102**, 223; b) G. R. Luckhurst, *Liq. Cryst.*, 2005, **32**, 1335.
17. D. A. Paterson, J. P. Abberley, W. T. A. Harrison, J. M. D. Storey, C. T. Imrie, *Liq. Cryst.*, 2017, **44**, 127.
18. N. Sebastián, D. O. López, B. Robles-Hernández, M. R. de la Fuente, J. Salud, M. A. Pérez-Jubindo, D. A. Dunmur, G. R. Luckhurst, D. J. B. Jackson, *Phys. Chem. Chem. Phys.*, 2014, **16**, 21391.
19. a) C. T. Archbold, J. L. Andrews, R. J. Mandle, S. J. Cowling, J. W. Goodby, *Liq. Cryst.*, 2017, **44**, 84; b) R. J. Mandle, C. T. Archbold, J. P. Sarju, J. L. Andrews, J. W. Goodby, *Sci. Rep.*, 2016, **6**, 36682; c) R. J. Mandle, E. J. Davis, C. T. Archbold, S. J. Cowling, J. W. Goodby, *J. Mater. Chem. C*, 2014, **2**, 556; d) R. J. Mandle, E. J. Davis, C.-C. A. Voll, C. T. Archbold, J. W. Goodby, S. J. Cowling, *Liq. Cryst.*, 2015, **42**, 688; e) R. J. Mandle, *Chem. Rec.*, 2018, **18**, 1.
20. D. A. Paterson, M. Gao, Y.-K. Kim, A. Jamali, K. L. Finley, B. Robles-Hernández, S. Diez-Berart, J. Salud, M. R. de la Fuente, B. A. Timimi, H. Zimmermann, C. Greco, A. Ferrarini, J. M. D. Storey, D. O. López, O. D. Lavrentovich, G. R. Luckhurst, C. T. Imrie, *Soft Matter*, 2016, **12**, 6827.
21. A. A. Dawood, M. C. Grossel, G. R. Luckhurst, R. M. Richardson, B. A. Timimi, N. J. Wells, Y. Z. Yousif, *Liq. Cryst.*, 2016, **43**, 2.
22. a) S. M. Jansze, A. Martínez-Felipe, J. M. D. Storey, A. T. M. Marcelis, C. T. Imrie, *Angew. Chem. Int. Ed.*, 2015, **54**, 643; b) R. Walker, D. Pocięcha, J. P. Abberley, A. Martínez-Felipe, D. A. Paterson, E. Forsyth, G. B. Lawrence, P. A. Henderson, J. M. D. Storey, E. Gorecka, C. T. Imrie, *Chem. Commun.*, 2018, **54**, 3383.
23. a) Y. Arakawa, Y. Sasaki, K. Igawa, H. Tsuji, *New J. Chem.*, 2017, **41**, 6514; b) Y. Arakawa, S. Inui, H. Tsuji, *Liq. Cryst.*, 2018, **45**, 811; c) Y. Arakawa, Y. Sasaki, N. Haraguchi, S. Itsuno, H. Tsuji, *Liq. Cryst.*, **45**, 821; d) Y. Arakawa, Y. Sasaki, H. Tsuji, *Chem. Lett.*, 2017, **46**, 1657; e) Y. Arakawa, H. Tsuji, *Mol. Cryst. Liq. Cryst.*, 2017, **647**, 422; h) Y. Arakawa, S. Kang, J. Watanabe, G. Konishi, *RSC Adv.*, 2015, **5**, 8056; g) Y. Arakawa, S. Kang, H. Tsuji, J. Watanabe, G. Konishi, *RSC Adv.*, 2016, **6**, 16568.
24. N. Miyaura, K. Yamada, A. Suzuki, *Tetrahedron Lett.*, 1979, **20**, 3437.
25. a) A. D. Becke, *J. Chem. Phys.*, 1993, **98**, 5648; b) P. J. Stephens, F. J. Devlin, C. F. Chabalowski, M. J. Frisch, *J. Phys. Chem.*, 1994, **98**, 11623.
26. Revision B.01, M. J. Frisch, G. W. Trucks, H. B. Schlegel, G. E. Scuseria, M. A. Robb, J. R. Cheeseman, G. Scalmani, V. Barone, G. A. Petersson, H. Nakatsuji, X. Li, M. Caricato, A. V. Marenich, J. Bloino, B. G. Janesko, R. Gomperts, B. Mennucci, H. P. Hratchian, J. V. Ortiz, A. F. Izmaylov, J. L. Sonnenberg, D. Williams-Young, F. Ding, F. Lipparini, F. Egidi, J. Goings, B. Peng, A. Petrone, T. Henderson, D. Ranasinghe, V. G. Zakrzewski, J. Gao, N. Rega, G. Zheng, W. Liang, M. Hada, M. Ehara, K. Toyota, R. Fukuda, J. Hasegawa, M. Ishida, T. Nakajima, Y. Honda, O. Kitao, H. Nakai, T. Vreven, K. Throssell, J. A. Montgomery, Jr., J. E. Peralta, F. Ogliaro, M. J. Bearpark, J. J. Heyd, E. N. Brothers,

## ARTICLE

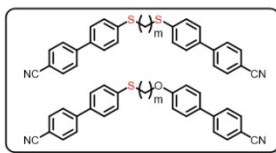
Journal Name

- 1  
2  
3 K. N. Kudin, V. N. Staroverov, T. A. Keith, R. Kobayashi, J.  
4 Normand, K. Raghavachari, A. P. Rendell, J. C. Burant, S. S.  
5 Iyengar, J. Tomasi, M. Cossi, J. M. Millam, M. Klene, C.  
6 Adamo, R. Cammi, J. W. Ochterski, R. L. Martin, K.  
7 Morokuma, O. Farkas, J. B. Foresman, D. J. Fox, Gaussian,  
8 Inc., Wallingford CT, 2016.
- 9 27. GaussView, Version 6, R. Dennington, T. A. Keith, J. M.  
10 Millam, Semichem Inc., Shawnee Mission, KS, 2016.
- 11 28. X. D. Li, S. K. Lee, S. Kang, M. Tokita, S. Kawauchi, J.  
12 Watanabe, *Chem. Lett.*, 2009, **38**, 424.
- 13 29. T. B. T. To, T. J. Sluckin, G. R. Luckhurst, *Phys. Chem. Chem.*  
14 *Phys.*, 2017, **19**, 29321-29332.
- 15 30. a) E. Gorecka, N. Vaupotič, A. Zep, D. Pocięcha, J. Yoshioka, J.  
16 Yamamoto, H. Takezoe, *Angew. Chem. Int. Ed.*, 2015, **54**,  
17 10155; b) Y. Wang, G. Singh, D. M. Agra-Kooijman, M. Gao, H.  
18 Krishna Bisoyi, C. Xue, M. R. Fisch, S. Kumar, Q. Li,  
19 *CrystEngComm*, 2015, **17**, 2778.
- 20 31. J. P. Jokisaari, G. R. Luckhurst, B. A. Timimi, J. Zhu, H.  
21 Zimmermann, *Liq. Cryst.*, 2015, **42**, 708;
- 22 32. Z. Zhang, V. P. Panov, M. Nagaraj, R. J. Mandle, J. W.  
23 Goodby, G. R. Luckhurst, J. C. Jones, H. F. Gleeson, *J. Mater.*  
24 *Chem. C*, 2015, **3**, 10007.
- 25 33. a) D. M. Agra-Kooijman, G. Singh, M. R. Fisch, M. R.  
26 Vengatesan, J.-K. Song, S. Kumar, *Liq. Cryst.*, 2017, **44**, 191;  
27 b) G. Singh, J. Fu, D. M. Agra-Kooijman, J.-K. Song, M. R.  
28 Vengatesan, M. Srinivasarao, M. R. Fisch, S. Kumar, *Phys.*  
29 *Rev. E*, 2016, **94**, 060701(R).
- 30 34. V. Borshch, Y.-K. Kim, J. Xiang, M. Gao, A. Ja'kli, V.P. Panov,  
31 J. K. Vij, C. T. Imrie, M. G. Tamba, G. H. Mehl, O.D.  
32 Lavrentovich, *Nat. commun.*, 2013, **4**, ncomms3635.
- 33 35. P. K. Challa, V. Borshch, O. Parri, C. T. Imrie, S. N. Sprunt, J. T.  
34 Gleeson, O. D. Lavrentovich, A. Jákli, *Phys. Rev. E*, 2014, **89**,  
35 060501(R).
- 36 36. a) Z. Ahmed, C. Welch, G. H. Mehl, *RSC Adv.*, 2015, **5**, 93513; b)  
37 K. Watanabe, T. Tamura, S. Kang, M. Tokita, *Liq. Cryst.*, 2018,  
38 **45**, 924.
- 39 37. C. Meyer, G. R. Luckhurst, I. Dozov, *J. Mater. Chem. C*, 2015,  
40 **3**, 318.
- 41 38. a) R. W. Taft Jr., I. C. Lewis, *J. Am. Chem. Soc.*, 1958, **80**, 2436;  
42 (b) D. H. McDaniel, H. C. Brown, *J. Org. Chem.*, 1958, **23**, 420;  
43 (c) C. Hansch, A. Leo, R. W. Taft, *Chem. Rev.*, 1991, **97**, 165.
- 44 39. a) P. Mach, R. Pindak, A.-M. Levelut, P. Barois, H. T. Nguyen, C.  
45 C. Huang, L. Furenlid, *Phys. Rev. Lett.*, 1998, **81**, 1015; b) L. S.  
46 Hirst, S. J. Watson, H. F. Gleeson, P. Cluzeau, P. Barois, R. Pindak,  
47 J. Pitney, A. Cady, P. M. Johnson, C. C. Huang, A.-M. Levelut, G.  
48 Srajer, J. Pollmann, W. Caliebe, A. Seed, M. R. Herbert, J. W.  
49 Goodby, M. Hird, *Phys. Rev. E*, 2002, **65**, 041705.
- 50  
51  
52  
53  
54  
55  
56  
57  
58  
59  
60

View Article Online  
DOI: 10.1039/C8NJ06456C

New Journal of Chemistry Accepted Manuscript

1  
2  
3  
4  
5  
6  
7  
8  
9  
10  
11  
12  
13  
14  
15  
16  
17  
18  
19  
20  
21  
22  
23  
24  
25  
26  
27  
28  
29  
30  
31  
32  
33  
34  
35  
36  
37  
38  
39  
40  
41  
42  
43  
44  
45  
46  
47  
48  
49  
50  
51  
52  
53  
54  
55  
56  
57  
58  
59  
60



**"Thioether"-linked twist-bend nematogens**  
with enhanced glass-forming ability

338x190mm (96 x 96 DPI)